

Absolute differential cross sections for low-energy He^{+}-He collisions via fully quantum dynamics

Yu Wang(王瑜), Kun Wang(王堃), Yu-Kun Yang(杨玉坤), Chuan-Liang Li(李传亮), Ling Liu(刘玲), Yong Wu(吴勇), Svetlana A. Yakovleva, and Andrey K. Belyaev

Citation: Chin. Phys. B, 2026, 35 (**7**): 073401. DOI: 10.1088/1674-1056/ae64d6
http://cpb.iphy.ac.cn; http://iopscience.iop.org/cpb

What follows is a list of articles you may be interested in

Charge transfer processes in low-energy Na^{+}-Na collisions

Cheng-Cheng Jiang(蒋承呈), Xiao-Xia Wang(王小霞), Kun Wang(王堃), Yi-Zhi Qu(屈一至), Jian-Guo Wang(王建国), Xia Li(李侠), Li Ma(马丽), and Robert J. Buenker

Chin. Phys. B, 2026, 35 (**4**): 043402. DOI: 10.1088/1674-1056/ae15f0

Single electron capture in low- and intermediate-energy collisions of $Si^{3,4+}$ with He

Yingzhou Li(李英卓), Yadong Liu(刘亚东), Yueying Qi(祁月盈), Ling Liu(刘玲), Yizhi Qu(屈一至), and Jianguo Wang(王建国)

Chin. Phys. B, 2026, 35 (**1**): 013401. DOI: 10.1088/1674-1056/ae15f4

Electron capture and excitation in intermediate-energy He^{2+}-H(1s,2s) collisions

Yadong Liu(刘亚东), Congcong Jia(贾聪聪), Mingxuan Ma(马茗萱), Xiang Gao(高翔), Ling Liu(刘玲), Yong Wu(吴勇), Xiangjun Chen(陈向军), and Jianguo Wang(王建国)

Chin. Phys. B, 2024, 33 (**8**): 083401. DOI: 10.1088/1674-1056/ad5322

Quantitative rescattering theory for nonsequential double ionization

Zhangjin Chen(陈长进), Fang Liu(刘芳), Hua Wen(文华)

Chin. Phys. B, 2019, 28 (**12**): 123401. DOI: 10.1088/1674-1056/ab54b3

Polarization and exchange effects in elastic scattering of electron with atoms and ions

Zhang-Jin Chen(陈长进), Dan-Dan Cui(崔丹丹)

Chin. Phys. B, 2018, 27 (**5**): 053403. DOI: 10.1088/1674-1056/27/5/053403

DATA PAPER

Absolute differential cross sections for low-energy He^+–He collisions via fully quantum dynamics

Yu Wang(王瑜)[1], Kun Wang(王堃)[2], Yu-Kun Yang(杨玉坤)[3], Chuan-Liang Li(李传亮)[1,†], Ling Liu(刘玲)[4,‡], Yong Wu(吴勇)[4], Svetlana A. Yakovleva[5], and Andrey K. Belyaev[5]

[1] *Shanxi Province Engineering Research Center of Precision Measurement and Online Detection Equipment, School of Applied Science, Taiyuan University of Science and Technology, Taiyuan* 030024, *China*

[2] *Institute of Environmental Science, Shanxi University, Taiyuan* 030006, *China*

[3] *School of Physics, Henan Normal University, Xinxiang* 453000, *China*

[4] *Key Laboratory of Computational Physics, Institute of Applied Physics and Computational Mathematics, Beijing* 100088, *China*

[5] *Department of Theoretical Physics and Astronomy, Herzen University, St. Petersburg* 191186, *Russia*

(Received 30 March 2026; revised manuscript received 16 April 2026; accepted manuscript online 27 April 2026)

Angular differential cross sections for elastic scattering and charge transfer in low-energy He^+–He collisions underpin diverse plasma applications, yet systematic quantum mechanical data remain scarce. Employing the fully quantum mechanical molecular-orbital close-coupling method with high-accuracy *ab initio* potential energy curves, absolute angular differential cross sections are computed over 0.005–1250 eV/u and scattering angles 0.01°–90°. The present results show good agreement with available high-resolution experimental benchmarks in both magnitude and oscillatory structure, with improved consistency over existing semiclassical and single-electron approaches. By decomposing the cross sections into separate symmetric and antisymmetric channel contributions, three classes of oscillatory structures and their energy evolution are identified: regular oscillations from two-channel quantum interference, irregular oscillations from rainbow scattering in the deep attractive well, and fine-scale oscillations from matter-wave diffraction off the repulsive wall. This work provides the first systematic, fully quantum mechanical differential cross-section dataset across the low-energy and full angular range, serving as reliable reference data for plasma modeling and related applications.

Keywords: elastic scattering, charge transfer, fully quantum dynamics, angular differential cross sections

PACS: 34.70.+e, 13.85.Dz, 82.20.Pm, 82.20.Ej

DOI: 10.1088/1674-1056/ae64d6 **CSTR:** 32038.14.CPB.ae64d6

1. Introduction

The He^+–He collision system is a prototypical symmetric scattering system in atomic collision physics, and its elastic scattering and charge transfer processes are of considerable interest in several important application fields. In fusion plasma research, when the plasma temperature in the region near the divertor target plates of tokamak devices such as ITER and DEMO falls below 40 eV, charge transfer reactions between helium ash and He^+/He^{2+} surpass the proton–helium system and become dominant.[1] In astrophysics, Wedlund *et al.*[2,3] pointed out in their study of the atmosphere of comet 67P/Churyumov-Gerasimenko that charge exchange between solar wind α particles and the cometary neutral atmosphere is the primary source of helium ions, which in turn drive cascading charge exchange reactions. Furthermore, Yousfi *et al.*[4,5] showed that elastic and inelastic collision parameters of He^+ with He and air molecules in atmospheric-pressure low-temperature plasma jets are crucial for understanding the formation and propagation mechanisms of ionization waves, a technology with broad prospects in biomedical remote treatment applications. These application scenarios establish a clear need for angular differential cross sections (DCS) data of elastic scattering and charge transfer in He^+–He collisions.

Substantial experimental and theoretical effort has been devoted to the angular DCS of this system. More broadly, recent work continues to highlight the importance of differential and state-resolved observables in ion–atom collision studies.[6,7]

On the experimental side, Lorents *et al.*[8] carried out pioneering measurements in the 10–300 eV/u and 1°–36° range, while Vestal *et al.*[9] measured DCS at lower energies of 0.12–7.55 eV/u up to 90° laboratory angle; however, both works were limited in angular resolution by the experimental conditions available at the time. Subsequently, Gao *et al.*[10] achieved high-angular-resolution measurements of absolute DCS in the 62.5–1250 eV/u and 0°–10° range, which remain the most reliable experimental benchmark data for this system to date. More recently, Guo *et al.*[11] employed recoil-ion momentum spectroscopy to measure DCS for charge transfer at

†Corresponding author. E-mail: clli@tyust.edu.cn

‡Corresponding author. E-mail: liu_ling@iapcm.ac.cn

© 2026 Chinese Physical Society and IOP Publishing Ltd. All rights, including for text and data mining, AI training, and similar technologies, are reserved.

7.5 keV/u and 25 keV/u, providing new experimental reference data for the high-energy regime. Overall, the existing experimental record lacks high-angular-resolution absolute DCS data below 62.5 eV/u.

On the theoretical side, Marchi and Smith[12] first applied a semiclassical two-state theory using the potential energy curves calculated by Reagan *et al.*[13] and Phillipson *et al.*[14] to compute elastic scattering DCS at 7.5–150 eV/u, but could only qualitatively describe the main structural features observed experimentally due to insufficient accuracy of the potential curves in the long-range region. Olson *et al.*[15] improved the agreement with experiment at 5 eV/u and 7.5 eV/u through parameterized potential curves combined with an iterative two-state theory, but also noted the extreme sensitivity of the DCS to the potential energy surface accuracy and the need for more precise structure calculations. The semiclassical JWKB results of Gao *et al.*[10] agreed well with their experimental data over 62.5–1250 eV/u. In a subsequent study,[16] Gao *et al.* qualitatively analyzed the origins of oscillatory structures in the small-angle region in terms of three physical effects: quantum interference between the gerade/ungerade (g/u) channels, rainbow scattering from the potential well, and matter-wave diffraction from the repulsive wall, but that analysis was confined to the 62.5–1250 eV/u energy range and the 0°–10° small-angle interval within a semiclassical framework. Zhao *et al.*[17] computed charge transfer DCS over the corresponding energy range using the single-electron two-center atomic orbital close-coupling (TC-AOCC) method; their results agreed with experiment at small scattering angles but showed increasingly significant deviations as the scattering angle increased. Regarding the physical mechanisms underlying the oscillatory structures in the DCS, Aberth *et al.*[18] and Olson *et al.*[15] confirmed with two-state theory that the regular oscillations originate from quantum interference between the g and u channel scattering amplitudes, while Barat *et al.*[19] experimentally revealed the role of ungerade state channel excitation in the disappearance of oscillatory structures at high energies and large angles.

From the above, it is evident that existing theoretical work has relied primarily on semiclassical approximations or single-electron models, while systematic fully quantum mechanical calculations remain lacking in the low-energy regime (<100 eV/u) and at large scattering angles, where experimental data are also scarce. For the symmetric He^+–He system, the interference between the gerade and ungerade channels plays a central role in shaping the fine oscillatory structures in the angular DCS. Recent developments in fully quantum treatments of low-energy ion–atom collisions have further underscored the need for approaches beyond semiclassical descriptions.[20,21] In this context, the molecular-orbital close-coupling (QMOCC) method is particularly suitable, as it rigorously treats the quantum scattering dynamics through partial-wave expansion and naturally accounts for the two-channel interference in symmetric collisions.

To address these theoretical limitations and provide high-accuracy benchmarks, a systematic fully quantum mechanical investigation is conducted in this work. Using high-accuracy He_2^+ potential energy curves previously obtained by the multi-reference single- and double-excitation configuration interaction (MRD-CI) method,[22] the QMOCC method is employed to systematically compute the absolute angular DCS for elastic scattering and charge transfer in $He^+(1s)$–$He(1s^2)$ collisions over the energy range 0.005–1250 eV/u and laboratory scattering angles from 0.01° to 90° (corresponding to the full 0°–180° center-of-mass range for this homonuclear system). The results are benchmarked against available experimental[8,10] and theoretical[10,15,17] data, and the separate g and u channel contributions are analyzed over the full angular range to elucidate the underlying physical mechanisms of the oscillatory structures.

2. Theoretical method

The theoretical framework and numerical implementation of the QMOCC method have been systematically described in Refs. [20,21,23–25]. This section outlines the core formulas relevant to the DCS calculation and specifies the computational parameters used in this work. Under the Born–Oppenheimer approximation, the QMOCC method expands the total wave function in adiabatic electronic states and reduces the three-dimensional scattering problem to a set of coupled radial equations via partial-wave expansion. These equations are solved numerically using the multichannel log-derivative method[26] to obtain the reaction matrix K, from which the scattering matrix S is constructed as

$$S_{ij,J} = \frac{\boldsymbol{I} + \mathrm{i}K_{ij,J}}{\boldsymbol{I} - \mathrm{i}K_{ij,J}}, \tag{1}$$

where $\boldsymbol{I}$ is the identity matrix and J is the total angular momentum quantum number.

For the He^+–He system, which consists of two identical nuclei, the electronic Hamiltonian possesses inversion symmetry. The total electronic wave function assumes either symmetric (gerade) or antisymmetric (ungerade) form under spatial inversion; the corresponding potential energy curves are shown in Fig. 1. Previous work[22] established that low-energy He^+–He charge transfer is dominated by the resonant channel associated with the two lowest states. The present treatment therefore retains only the two lowest adiabatic states of He_2^+, $X\,^2\Sigma_u^+$ and $A\,^2\Sigma_g^+$. Owing to their different inversion symmetries, these states are dynamically decoupled, so that each reduces to a single-channel scattering problem. The second dissociation limit, $He^+(1s)$ + $He(1s2s\ ^1S)$, lies 19.820 eV above the ground entrance channel $He^+(1s)$ + $He(1s^2)$, which closes

the corresponding excited channels below 9.91 eV/u. Moreover, Ref. [22] showed from 34-state QMOCC calculations that, even at higher energies, transfer to excited states remains 2–3 orders of magnitude smaller than the dominant ground-state resonant channel. The two-state approximation adopted here is therefore well justified for the present DCS analysis.

Accordingly, the S matrix in Eq. (1) reduces to a scalar S_J^g or S_J^u for the respective symmetry. The scattering amplitude in each channel takes the unified form[24]

$$f^{g,u}(E,\theta) = \frac{1}{2ik}\sum_{J=0}^{J_{\max}}(2J+1)\left(1-S_J^{g,u}\right)P_J(\cos\theta), \qquad (2)$$

where k is the initial center-of-mass momentum and P_J denotes the Legendre polynomial of degree J.

Assuming the initial collision state is $[\mathrm{He}_A^+ + (\mathrm{He}_B^+ + e)]$, the corresponding wave function can be represented by the radial function $[\psi_g(R)+\psi_u(R)]/2$. Elastic scattering leaves the channel unchanged, so that its scattering amplitude is the sum of the g and u channel amplitudes; charge transfer corresponds to the final channel $[(\mathrm{He}_A^+ + e) + \mathrm{He}_B^+]$, obtained from $[\psi_g(R)-\psi_u(R)]/2$. The effective S matrices for the two processes are therefore[24]

$$S_J^{\mathrm{el}} = \frac{1}{2}\left(S_J^g + S_J^u\right), \quad S_J^{\mathrm{ct}} = \frac{1}{2}\left(S_J^g - S_J^u\right), \qquad (3)$$

where the superscripts el and ct denote elastic scattering and charge transfer, respectively.

For elastic scattering, the absolute angular DCS is

$$\frac{\mathrm{d}\sigma^{\mathrm{el}}}{\mathrm{d}\Omega} = \frac{1}{4k^2}\left|\sum_{J=0}^{J_{\max}}(2J+1)\left(1-S_J^{\mathrm{el}}\right)P_J(\cos\theta)\right|^2, \qquad (4)$$

while for charge transfer, where the electron is transferred between two equivalent nuclei so that the initial and final channels differ despite identical energy levels, the DCS is

$$\frac{\mathrm{d}\sigma^{\mathrm{ct}}}{\mathrm{d}\Omega} = \frac{1}{4k^2}\left|\sum_{J=0}^{J_{\max}}(2J+1)\,S_J^{\mathrm{ct}}\,P_J(\cos\theta)\right|^2. \qquad (5)$$

Integrating Eqs. (4) and (5) over the full solid angle yields the total integral cross sections for elastic scattering and charge transfer, respectively. For this homonuclear collision system, the laboratory frame scattering angle θ_{lab} is related to the center-of-mass angle by $\theta_{\mathrm{cm}} = 2\theta_{\mathrm{lab}}$. Thus, the laboratory angular range 0°–90° corresponds to the full 0°–180° range in the center-of-mass frame. Throughout this paper, scattering angles refer to the laboratory frame unless stated otherwise.

The present calculations use the high-accuracy He_2^+ potential energy curves obtained by the MRD-CI *ab initio* method in Ref. [22], as shown in Fig. 1. For the $\mathrm{X}^2\Sigma_u^+$ state, the well depth and equilibrium internuclear distance are $D_e = 2.458$ eV and $R_e = 2.052\ a_0$, respectively, while for the $\mathrm{A}^2\Sigma_g^+$ state they are $D_e = 0.003$ eV and $R_e = 8.668\ a_0$. These values are consistent with previous theoretical and spectroscopic data; a detailed comparison is given in Ref. [22]. In particular, the present D_e and R_e for the deep $\mathrm{X}^2\Sigma_u^+$ state differ from earlier values by less than about 0.6% and 0.5%, respectively. For the shallow $\mathrm{A}^2\Sigma_g^+$ state, although the present well depth is somewhat larger than earlier results, the absolute difference is only about 0.001 eV and the deviation in R_e remains below 1%. Because this minimum is only of order 10^{-3} eV, its exact depth is especially sensitive to the details of the electronic-structure treatment.

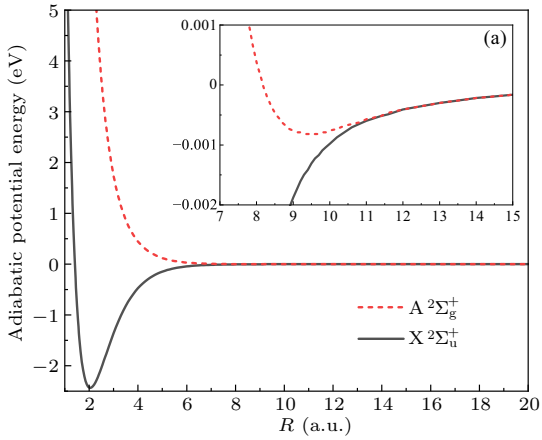


Fig. 1. Adiabatic potential energy curves of the two lowest states $\mathrm{X}^2\Sigma_u^+$ (ungerade) and $\mathrm{A}^2\Sigma_g^+$ (gerade) of He_2^+. The inset shows the shallow well of the $\mathrm{A}^2\Sigma_g^+$ state in the long-range region.

In the fully quantum-dynamical calculation, the log-derivative propagation is carried out from $R_{\min} = 0.5a_0$ to $R_{\max} = 500a_0$ with a step size of $0.0001a_0$. The partial-wave truncation $J_{\max}$ increases substantially with collision energy: convergence is achieved at $J_{\max} \approx 150$ for 0.005 eV/u, rising to $J_{\max} \approx 12000$ at 1250 eV/u. To assess the reliability of the present dataset, convergence tests were carried out with respect to the radial propagation range, propagation step size, and the partial-wave truncation $J_{\max}$. At each collision energy, $J_{\max}$ was increased until the DCS changed by less than 0.01% over the angular range of interest, so that the numerical uncertainty associated with the scattering propagation itself is very small. The remaining uncertainty is expected to arise mainly from the quality of the underlying *ab initio* potential energy curves, particularly in regions where the DCS is highly sensitive to phase differences between the g and u channels or to the details of the shallow long-range minimum of the $\mathrm{A}^2\Sigma_g^+$ state.

3. Results and discussion

Using the QMOCC method described in Section 2, systematic computations of the absolute angular DCS for elastic scattering and charge transfer in $\mathrm{He}^+(1s)$–$\mathrm{He}(1s^2)$ collisions are performed over the energy range 0.005–1250 eV/u and scattering angles 0.01°–90°. To validate the computational

scheme, a comparison with available experimental and theoretical data is first carried out in the 0.01°–10° range.

Figure 2 shows the absolute DCS for charge transfer at collision energies of 7.5 eV/u, 62.5 eV/u, 125 eV/u, 375 eV/u, 625 eV/u, and 1250 eV/u, compared with the experimental measurements and JWKB calculations of Gao *et al.*,[10] as well as the TC-AOCC results of Zhao *et al.*[17] Over the entire energy range, the QMOCC results show better overall agreement with the experimental data[10] than either of these two methods. At the higher energies of 625 eV/u and 1250 eV/u, both QMOCC and JWKB reproduce the experimental data reasonably well in terms of the overall magnitude and oscillatory structure. Nevertheless, the present QMOCC results follow the experimental points somewhat more closely in several local features, especially over approximately 0.1°–0.3° in panel (e) at 625 eV/u, where a representative comparison gives relative deviations of about 8.6% for QMOCC and 46.1% for JWKB, as well as over approximately 0.08°–0.3° in panel (f) at 1250 eV/u, where the peak intensities and overall oscillatory profile are reproduced more faithfully.

By contrast, the TC-AOCC method[17] agrees with experiment at small scattering angles but develops progressively larger deviations as the scattering angle increases. This systematic discrepancy is likely related to the single-electron approximation and the associated technical treatments adopted in TC-AOCC, such as basis-set incompleteness and the choice of electron translation factors, which limit its ability to reproduce the full oscillatory behavior across the angular range. The QMOCC calculations successfully reproduce the oscillatory structures observed experimentally at all energies. At 7.5 eV/u [Fig. 2(a)], which lies below the range covered by Gao *et al.*,[10] no directly comparable experimental or JWKB data are available for charge-transfer DCS. Although the low-energy measurements of Vestal *et al.*[9] extend to this energy range, they do not provide angle-resolved charge-transfer DCS and therefore are not included in Fig. 2. The present result therefore provides a useful fully quantum-mechanical reference for the charge-transfer DCS in this low-energy regime.

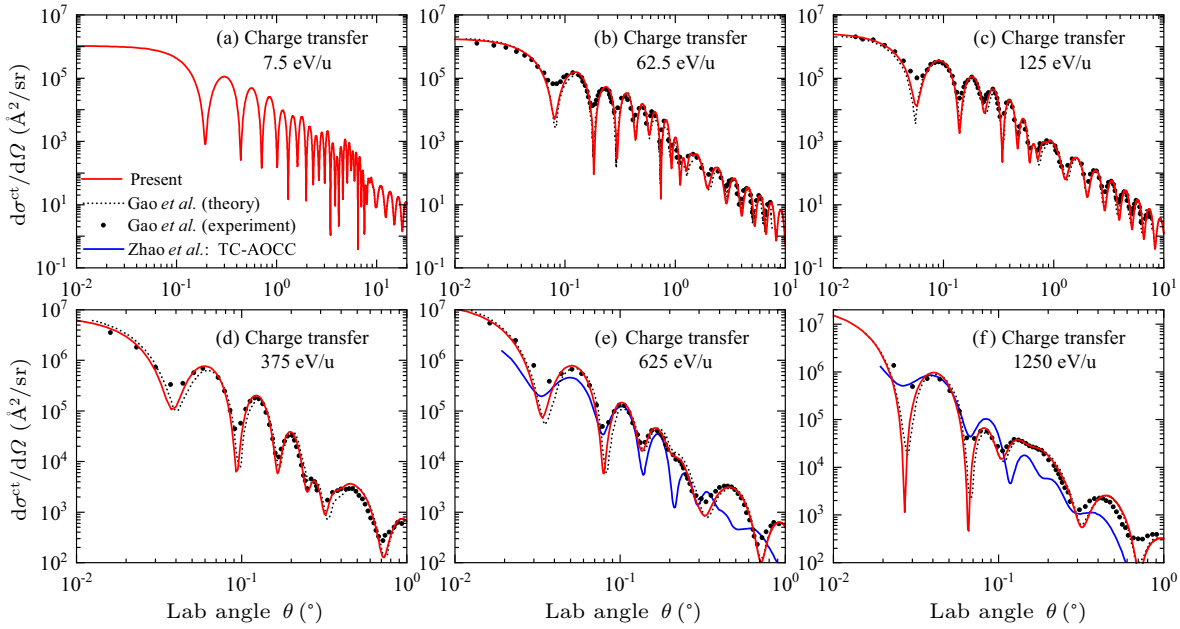


Fig. 2. Absolute DCS for charge transfer in $He^+(1s)$–$He(1s^2)$ collisions at energies of 7.5 eV/u (a), 62.5 eV/u (b), 125.0 eV/u (c), 375.0 eV/u (d), 625.0 eV/u (e) and 1250.0 eV/u (f). Red solid line: present QMOCC results; blue solid line: TC-AOCC results of Zhao *et al.*;[17] black dotted line: JWKB results of Gao *et al.*;[10] black dots: experimental results of Gao *et al.*[10]

Figure 3 shows the absolute DCS for elastic scattering at the same energies. At 7.5 eV/u, the present results are compared with the available two-state theoretical results of Marchi *et al.*[12] and Olson *et al.*,[15] as well as the experimental data of Lorents *et al.*[8] and Vestal *et al.*[9] The QMOCC method provides higher angular resolution at small angles, and the overall oscillatory trend is consistent with the results of Olson *et al.*[15] The results of Marchi *et al.*[12] exhibit a clear phase shift in the oscillations due to insufficient accuracy of their potential energy curves in the long-range region, whereas Olson *et al.*[15] improved the potentials through parameter fitting, bringing the large-angle extrema into agreement with the experiments of Lorents *et al.*[8] The comparison with the low-energy experimental data of Vestal *et al.*[9] is necessarily qualitative because of their limited angular resolution, but the present QMOCC results remain broadly consistent with the available experimental trend in the overlapping angular range, which further supports the reliability of the calculation at 7.5 eV/u.

At 375 eV/u, the QMOCC results agree well with the high-resolution experimental data and JWKB values of Gao *et al.*[10] over the entire angular range, further confirming the reliability of the present computational scheme. For the remaining energies (62.5 eV/u, 125 eV/u, 625 eV/u, and 1250 eV/u),

no other elastic scattering theoretical or experimental data have been published; the present QMOCC predictions can serve as a reference for future experimental verification. The reliability of the present scheme is further supported at the level of integral cross sections: in previous work,[22] elastic scattering and charge transfer total integral cross sections computed with the same potential energy curves and QMOCC method showed good agreement with available experimental and theoretical data over the broad range 0.005–2500 eV/u. Together with the present agreement with the available differential experimental benchmarks in Figs. 2 and 3, this provides important external support for the overall reliability of the present DCS dataset.

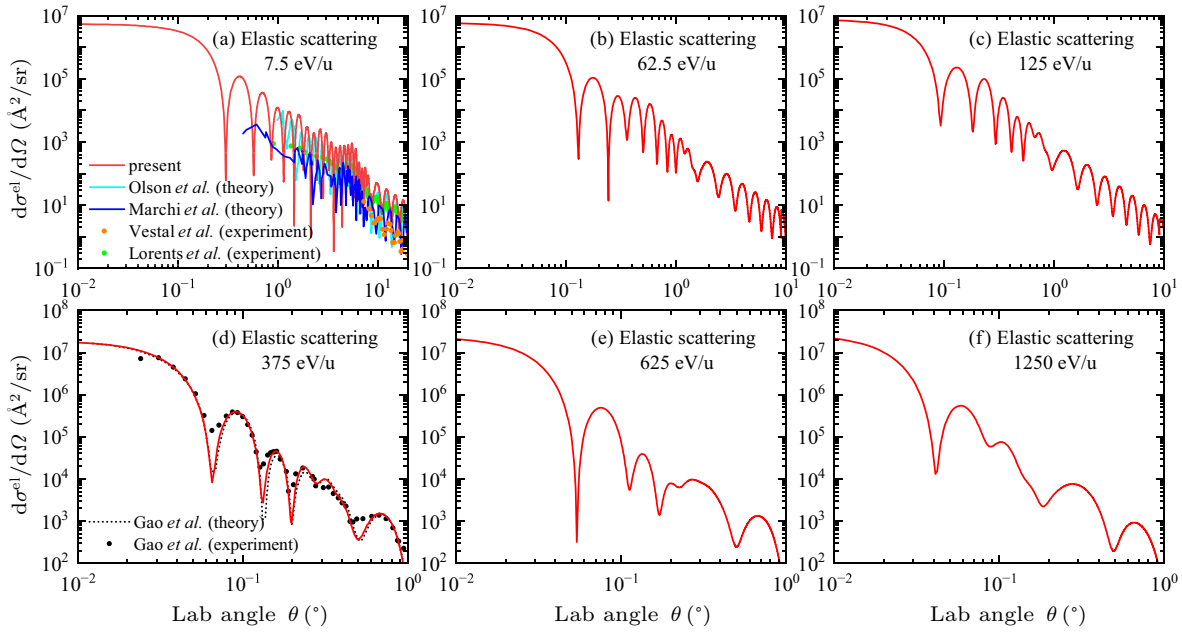


Fig. 3. Absolute DCS for elastic scattering in $He^+(1s)$–$He(1s^2)$ collisions at energies of 7.5 eV/u (a), 62.5 eV/u (b), 125 eV/u (c), 375 eV/u (d), 625 eV/u (e) and 1250 eV/u (f). Red solid line: present QMOCC results; black dotted line: JWKB results of Gao *et al.*;[10] cyan solid line: iterative two-state results of Olson *et al.*;[15] blue solid line: two-state results of Marchi *et al.*;[12] green dots: experimental results of Lorents *et al.*;[8] orange dots: experimental results of Vestal *et al.*;[9] black dots: experimental results of Gao *et al.*[10]

To gain deeper insight into the oscillatory structures and their energy dependence, Fig. 4 presents the DCS for charge transfer and elastic scattering at collision energies of 0.005 eV/u, 0.05 eV/u, 0.5 eV/u, 5 eV/u, 50 eV/u, and 500 eV/u, together with the DCS computed separately from the $X^2\Sigma_u^+$ (u) and $A^2\Sigma_g^+$ (g) potential channels. For visual clarity, the individual g and u channel results are multiplied by a factor of 10. The left and right columns use logarithmic and linear horizontal axes, respectively, covering the full 0.01°–90° angular range. Gao *et al.*[10,16] previously attributed the oscillatory structures in the small-angle regime (0–10°) at 62.5–1250 eV/u to three effects within a semiclassical framework: g/u channel interference, rainbow scattering, and matter-wave diffraction. The present fully quantum mechanical calculations, by decomposing the DCS into separate channel contributions over the full angular range, advance this classification to a quantitative level and reveal, for the first time, the complete energy evolution of these three mechanisms across five orders of magnitude in collision energy.

Three distinct classes of oscillatory structure can be identified from the channel-decomposed DCS. The most prominent is the g/u channel interference. Because the effective S matrices for elastic scattering and charge transfer are the symmetric and antisymmetric combinations of S^g and S^u [Eq. (3)], the phase-shift difference accumulated in the two channels produces regular oscillations whose period increases approximately linearly with scattering angle. These oscillations become progressively more distinct above 5 eV/u and dominate the intermediate angular range (approximately 13°–70° at 5 eV/u, 2°–70° at 50 eV/u, and 0.6°–8° at 500 eV/u), with the onset angle shifting to smaller values as the collision energy increases.[18,27] A direct signature is the strictly complementary oscillation between the elastic and charge transfer DCS: at all energies, each peak in one channel corresponds precisely to a valley in the other.

The second class of oscillation arises from rainbow scattering in the deep u-state well ($D_e \approx 2.458$ eV). The attractive potential bends trajectories with different impact parameters toward the same deflection angle, producing an extremum in the deflection function at the rainbow angle θ_r.[28,29] This is most clearly seen in the u-channel DCS at 5 eV/u [Fig. 4(d)], where two superimposed oscillation patterns appear below $\theta_r \approx 9°$: oscillations with large angular separation constitute the rainbow structure proper, with the first maximum near

θ_r being the primary rainbow and the subsidiary maxima at smaller angles being the supernumerary rainbows, while oscillations with small angular separation are superimposed on them, arising from the interference between partial waves associated with the far-side branch of the deflection function and those near the rainbow turning point.[29] Beyond θ_r, only one classical trajectory contributes and the cross section decays monotonically. At the lowest energies (0.005–0.5 eV/u), the collision energy lies below the well depth; incident particles undergo orbiting and large-angle deflection, and the resulting irregular oscillations pervade the entire 0–90° range, as seen in the u-channel DCS of Figs. 4(a)–4(c). With increasing energy, θ_r retreats toward the forward direction and the rainbow features become progressively less distinct as the collision energy far exceeds the well depth.

The third class, matter-wave diffraction off the repulsive core, produces fine-scale oscillations most clearly visible in the g-channel DCS at 500 eV/u [Fig. 4(f)], where the extremely shallow g-state well ($D_e \approx 0.003$ eV) is insufficient to produce rainbow scattering. A small oscillation near 0.05° and similar patterns shared by the g and u channels in the 3°–9° range are consistent with this mechanism: large-angle scattering is dominated by close collisions at small impact parameters, where the two potentials are nearly indistinguishable, so the diffraction patterns in the two channels naturally coincide. Gao *et al.*[16] similarly attributed such small-angle undulations to repulsive-wall diffraction.

Over the full angular range, the rate at which the DCS decreases with angle depends strongly on the collision energy. On the logarithmic axis, both the charge transfer and elastic scattering DCS exhibit a forward plateau, a region of approximately constant cross section near the smallest angles, whose value rises and angular extent narrows with increasing energy, following the scaling $\theta_1 \propto E^{-1/2}$ of the first oscillation peak position. At the low-energy end (0.005–0.5 eV/u), the DCS drops by only 2–4 orders of magnitude across the entire range, with oscillatory structures extending to near 90°; this slow angular attenuation is directly relevant to low-temperature plasma applications, such as the divertor region of fusion devices,[1] where large-angle scattering contributes non-negligibly to momentum transfer. At higher energies, the DCS falls steeply beyond the rainbow region: at 500 eV/u a drop of nearly 4 orders of magnitude occurs over approximately 5°–15°, consistent with the classical deflection function,[29] which severely restricts large-angle scattering when the collision energy far exceeds the well depth.

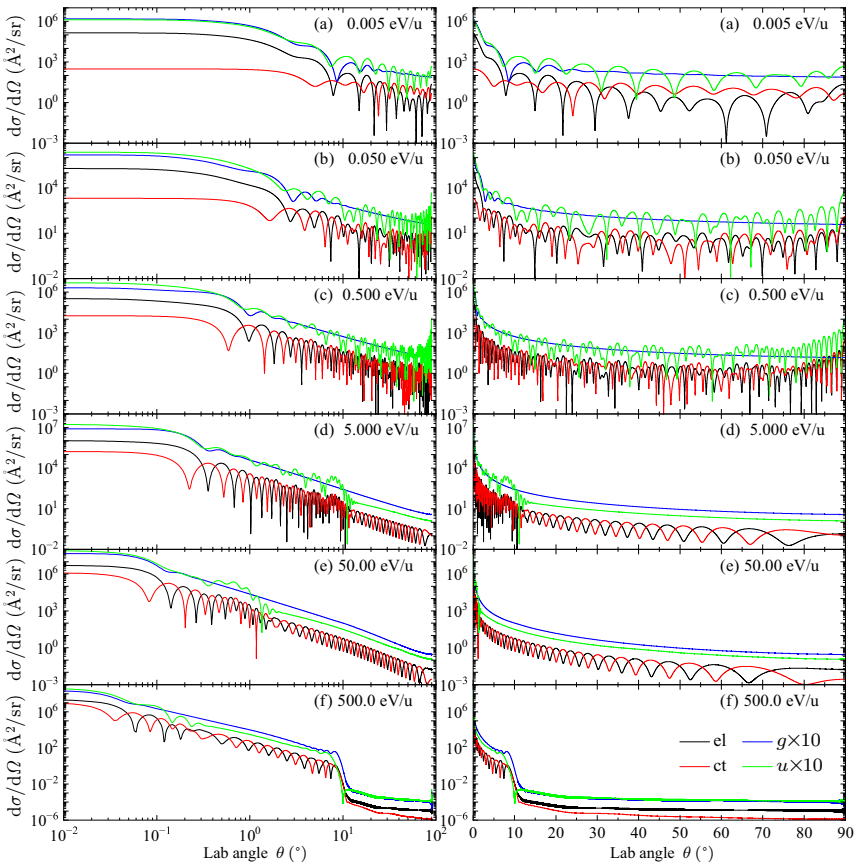


Fig. 4. DCS for charge transfer (ct), elastic scattering (el), and contributions from the gerade (g) and ungerade (u) potential channels separately in $He^+(1s)$–$He(1s^2)$ collisions at energies of 0.005 eV/u (a), 0.050 eV/u (b), 0.500 eV/u (c), 5.000 eV/u (d), 50.000 eV/u (e) and 500.000 eV/u (f). For visual clarity, the g and u channel results are multiplied by a factor of 10. Left column: logarithmic horizontal axis; right column: linear horizontal axis.

4. Conclusions

Using the QMOCC method together with high-accuracy *ab initio* MRD-CI potential energy curves of He_2^+, a systematic fully quantum-mechanical study of absolute angular differential cross sections (DCS) for elastic scattering and charge transfer in He^+–He collisions is presented over the energy range 0.005–1250 eV/u and scattering angles 0.01°–90°. Where high-resolution experimental benchmarks are available, the QMOCC results agree well with measurements in both magnitude and oscillatory structure, showing improved overall consistency compared with the JWKB approximation and the TC-AOCC method. The systematic deviations of TC-AOCC at large scattering angles confirm the inadequacy of the single-electron approximation and its associated technical treatments for this system. By decomposing the DCS into *g* and *u* channel contributions over the full angular range, this work advances the oscillatory-mechanism taxonomy of Gao *et al.* from a semiclassical qualitative framework to a fully quantitative level, revealing the complete energy evolution of the three classes of oscillatory structures: regular complementary oscillations from *g*/*u* quantum interference, prominent at intermediate and higher energies; irregular oscillations from rainbow scattering in the deep *u*-state well, pervading the full angular range at low energies and retreating toward the forward direction as the energy increases; and fine-scale oscillations from repulsive-wall diffraction within individual channels. The full-angle calculations further reveal that at low energies the DCS attenuates only slowly with angle, indicating that large-angle scattering contributes non-negligibly to momentum transfer under low-temperature plasma conditions. The low-energy DCS data provided here fill a gap where neither experiments nor full quantum mechanical calculations previously existed, and can serve as reference data for collisional modeling in fusion divertor plasmas, cometary atmospheres, and atmospheric-pressure plasma jets. The numerical convergence of the scattering calculations, together with the good agreement obtained with the available differential and integral benchmark data, supports the use of the present results as a reliable DCS reference dataset for low-energy He^+–He collisions.

Data availability statement

The data presented in this paper are openly available in Science Data Bank at https://doi.org/10.57760/sciencedb.30583.

Acknowledgements

This work was supported by the National Natural Science Foundation of China (Grant Nos. 12504297, 12274040, 12304279, 12204288, and 62475182), the National Key R&D Program of China (Grant No. 2022YFA1602504), the Shanxi Province Scientific Research Initial Funding (Grant No. 20252011), and the Taiyuan University of Science and Technology Scientific Research Initial Funding (Grant No. 20242149). AKB gratefully acknowledges support by the internal grant of Herzen University (the Russian Federation), Project No. 46-VG.

References

[1] Deng B Q, Xie Z Y, Shi H W, Abou-gabal H H and Emmert G A 1993 *Contrib. Plasma Phys.* **33** 35
[2] Wedlund C S, Kallio E, Alho M, Nilsson H and Gronoff G 2016 *Astron. Astrophys.* **587** A154
[3] Wedlund C S, Behar E, Kallio E, Nilsson H, Alho M, Gunell H, Bodewits D, Beth A, Gronoff G and Hoekstra R 2019 *Astron. Astrophys.* **630** A36
[4] Yousfi M, Eichwald O, Merbahi N and Jomaa N 2012 *Plasma Sources Sci. Technol.* **21** 045003
[5] Yousfi M, Hennad A and Benhenni M 2007 *J. Phys. D: Appl. Phys.* **40** 1751
[6] Cui S C, Xing D D, Zhu X L, Su M G, Gao Y, Guo D L, Zhao D M, Zhang S F, Fu Y B and Ma X W 2024 *Chin. Phys. B* **33** 073401
[7] Mondal M, Mandal B, Mistry T, Jana D and Purkait M 2024 *Chin. Phys. B* **33** 113401
[8] Lorents D C and Aberth W 1965 *Phys. Rev.* **139** A1017
[9] Vestal M L, Blakley C R and Futrell J H 1978 *Phys. Rev. A* **17** 1321
[10] Gao R S, Johnson L K, Schafer D A, Newman J H, Smith K A and Stebbings R F 1988 *Phys. Rev. A* **38** 2789
[11] Guo D L, Ma X, Zhang R T, Zhang S F, Zhu X L, Feng W T, Gao Y, Hai B, Zhang M, Wang H B and Huang Z K 2017 *Phys. Rev. A* **95** 012707
[12] Marchi R P and Smith F T 1965 *Phys. Rev.* **139** A1025
[13] Reagan P N, Browne J C and Matsen F A 1963 *Phys. Rev.* **132** 304
[14] Phillipson P E 1962 *Phys. Rev.* **125** 1981
[15] Olson R E and Mueller C R 1967 *J. Chem. Phys.* **46** 3810
[16] Gao R S, Dutta C M, Lane N F, Smith K A, Stebbings R F and Kimura M 1992 *Phys. Rev. A* **45** 6388
[17] Zhao G P, Liu L, Chang Z, Wang J G and Janev R K 2018 *J. Phys. B: At. Mol. Opt. Phys.* **51** 085201
[18] Aberth W, Lorents D C, Marchi R P and Smith F T 1965 *Phys. Rev. Lett.* **14** 776
[19] Barat M, Brenot J C and Pommier J 1973 *J. Phys. B: At. Mol. Phys.* **6** L105
[20] Wang Y, Gong T, Li C, Wang K, Yang Y, Liu L, Liu J, Fiser B, Yakovleva S A, Wu Y, Wang J and Belyaev A K 2026 *Chin. Phys. Lett.* **43** 020303
[21] Lin X, Lin M J, Wang K, Wu Y, Ren Y, Wang Y and Li J 2025 *Acta Phys. Sin.* **74** 152501 (in Chinese)
[22] Wang Y, Wang F, Lin X, Liu L, Wu Y and Wang J 2023 *Astron. Astrophys.* **674** A201
[23] Zygelman B, Cooper D L, Ford M J, Dalgarno A, Gerratt J and Raimondi M 1992 *Phys. Rev. A* **46** 3846
[24] Bransden B H and McDowell M R C 1992 *Charge Exchange and the Theory of Ion-Atom Collisions* (Oxford: Oxford University Press) pp. 90–131
[25] Nolte J L, Stancil P C, Liebermann H P, Buenker R J, Hui Y and Schultz D R 2012 *J. Phys. B: At. Mol. Opt. Phys.* **45** 245202
[26] Johnson B R 1973 *J. Comput. Phys.* **13** 445
[27] Mittmann H U and Weise H P 1974 *Z. Naturforsch. A* **29** 400
[28] Ford K W and Wheeler J A 1959 *Ann. Phys.* **7** 259
[29] Bernstein R B (ed) 1979 *Atom-Molecule Collision Theory: A Guide for the Experimentalist* (New York: Plenum) p. 125